25th ABCM International Congress of Mechanical Engineering
October 20-25, 2019, Uberlândia, MG, Brazil

COB-2019-0951
THE FLOW OVER A CANTILEVER FINITE-HEIGHT SEMI-CIRCULAR CYLINDER WITH ASPECT RATIO 2

Evelyn Natalie Aguiar de Almeida
Aluisio Viais Pantaleão
São Paulo State University (Unesp), School of Engineering, Ilha Solteira
e-mail: evelyn.natalie.almeida@gmail.com
e-mail: aluisio.pantaleao@unesp.br

Odenir de Almeida
Experimental Aerodynamics Research Center, Federal University of Uberlandia, MG
e-mail: odenir.almeida@ufu.br

Abstract. *The flow over a cantilever (surface mounted) finite-height semi-circular cylinder with aspect ratio AR = 2 was studied by means of experimental and numerical tools. The experiments were carried out in a low-speed wind tunnel through measurements of drag-coefficient, local pressure distribution in the surfaces of the cylinder, and wake's velocity profile evaluation/visualization. All gathered results were used to validate a numerical approach by means of steady RANS with k-ω SST turbulence model. This is an ongoing partnership-research about the flow over cylinders with finite-height by using existing experimental and numerical capabilities from two distinct laboratories which will allow the characterization of the flow over such geometries shedding light to important aspects such as aerodynamic force and wake flow pattern. The results were satisfactory at the time of this investigation and allowed to establish future direction for this study and consequently new approaches for tackling this problem.*

Keywords: *finite-height semi-circular cylinder, low-speed wind tunnel, RANS.*

1. INTRODUCTION

Several schematics or models of a flow over a finite-height circular cylinder are presented in the literature, since this geometric shape can be a satisfactory approximation of buildings, cooling towers, fuel, gas systems and aerodynamics of numerous engineering applications. However, it is verified that there are rare or nonexistent studies on the flow around a finite-height semi-circular cylinder and the effect of the several variables on the flow around this bluff body, such as Reynolds number, and the aspect ratio - height over diameter (H/D).

The geometry of a finite-height semi-circular cylinder can be used to represent a vehicular side-view mirror, for instance. The importance of studying the flow behavior around this geometry is to obtain an aerodynamically efficient exterior design for drag reduction, which reflects in the reduction of fuel, an important element for vehicles nowadays, due to increased fuel prices and tougher government regulation on emissions of greenhouse gases.

As mentioned, in the literature there are not many references to the flow around a semi-circular cylinder, however as this geometry derives from a circular cylinder, thus it is assumed the flow behavior to be like the flow around a circular cylinder. At a sufficiently high Reynolds number, the flow around a bluff body is characterized by a large region of separated flow which leads to the formation of a sizeable wake downstream. The wake of a surface-mounted finite-height circular cylinder and the associated vortex patterns are strongly dependent on the cylinder aspect ratio and the thickness of the boundary layer on the ground plane relative to the dimensions of the cylinder, (Sumner, 2013).

A schematic of the flow around a surface-mounted finite-height semi-circular cylinder is shown in Fig. 1, of diameter D and height H, where x is the cross-stream coordinate, y is the vertical coordinate and z is the streamwise coordinate. As shown, the cylinder is mounted normal to a ground plane, where U(z) is the incoming mean flow velocity profile, U_∞ is the freestream velocity outside the boundary layer on the ground plane, and δ is the thickness of the boundary layer.

The flow field around a circular cylinder with aspect ratio ≥ 2, is characterized by the horseshoe vortex forming upstream at the cylinder-wall junction, (Kawamura et al., 1984), (Adaramola et al., 2006), (Johnston and Wilson, 1997). The wake of the finite circular cylinder is influenced by several parameters, such as the cylinder aspect ratio, the velocity of the flow, Reynolds number and the relative thickness of the boundary layer on the ground plane.

For an aspect ratio of 2, the same used in this study, but for a circular cylinder, (Frederich et al., 2007) obtained a model based on numerical simulations at Reynolds number 10^5, that shows side-tip vortices merged into the recirculation region, and trailing vortices arise downstream of the near-wake recirculation zone. Likewise, the flow behavior, mean static pressure distribution the pressure also strongly depends a lot on the aspect ratio, as reported in several studies for various aspect ratios and boundary layer thicknesses (Elbatran, 2016); (Pattenden et al., 2005). For low aspect ratio cylinders, the point of most negative pressure is located at the region of reverse flow, this pressure becomes more negative as the aspect ratio increases, (Tsutsui, 2012).

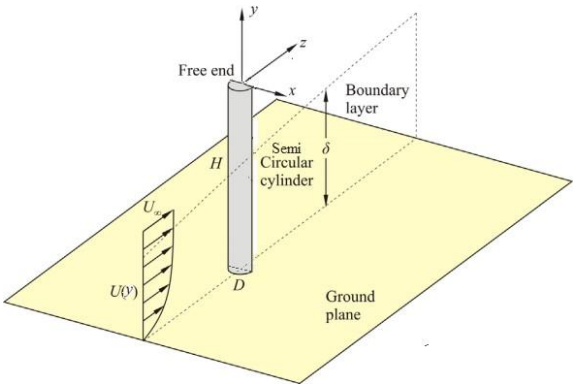

Figure 1. Schematic of the flow around a surface-mounted finite-height semi-circular cylinder. Adapted from (Sumner, 2013).

Most of studies presented in literature of a circular cylinder, agree on the basic elements of the mean flow field on the free-end surface, separation of the approach flow from the circumferential leading edge of the free-end surface; formation of mean recirculation zone on the free-end surface; reattachment of the separated flow onto the free-end surface along a prominent reattachment line; a reattachment saddle point on the centerline (Sumner, 2013). As the geometry studied in this work derives from a circular cylinder, it is expected some of the elements presents in the flow to be like the one around a circular cylinder.

This work is an ongoing research about the flow around a cantilever finite-height semi-circular cylinder with aspect ratio of 2, by employing existing measuring techniques/methodologies from two distinct research laboratories from Federal University of Uberlândia (UFU) and School of Engineering (FEIS-UNESP), through RANS (Reynolds Averaged Simulations) – numerical approach via Computational Fluid Dynamics (CFD) and physical (or material) experimentation by using a low-speed wind tunnel tests for the quantification of variables of interest and qualification of the flow (visualization) around such geometry. This collaboration work has been established as a basis to evaluate tools, methods and to provide means of studying the flow over finite-height cylinders. The results presented in this work are preliminary data obtained from this effort.

2. EXPERIMENTAL APPROACH

The experiments were carried out in the 60 x 60 cm^2 wind tunnel (TV-60) in the Experimental Aerodynamics Research Center (CPAERO) from Federal University of Uberlandia, Brazil, shown in Fig. 2. The drive system of the wind tunnel comprises a 12-blade rotor driven by a 25 HP electrical engine. The flow velocity is driven by an electrical inverter which output varies from 0 to 60 Hz, which gives a flow velocity range from 0 to 28 m/s. This subsonic wind tunnel is instrumented with Pitot tube, digital manometer, 3-component aerodynamic balance and other accessories such as hot-wire anemometers and smoke-visualization machine.

Figure 2. Wind Tunnel test facility (TV-60) - CPAERO.

Quantitative flow analysis was performed with a hot-wire anemometry system. The hot-wire anemometry is used to produce velocity profiles upstream and downstream the model. All measurements are performed using DANTEC Dynamics StreamLine Pro Anemometer System. A 1D hot-wire probe (55P11) is attached to a straight support and connected to one of the constant temperature anemometer (CTA) modules of the StreamLine Pro frame. The acquisition module is connected to a National Instruments A/D converter which sends data to the computer via a USB port. The system control and data exporting are done with the manufacturer's software, StreamWare Pro.

At the time of this study, the hot-wire anemometer was used to evaluate the boundary layer profile upstream the wall-mounted, finite-height semi-circular cylinder. The probe was positioned upstream the model at the location x/D = 2. Later, it is expected that cross-sectional lines could be established at different locations behind the cylinder and velocity measurements would be taken for each probe-position. For the boundary layer, the probe was moved from 2 to 2 mm and a total of 14 measures were taken. The sampling frequency was 2 kHz for a total of N = 32,768 sample points.

The test-article used in this study was made of Polyvinyl Chloride (PVC) with the insertion of two halves semi-circular wood to become the ceiling and base for the semi-circular cylinder having a radius of 50 mm. The semi-circular body was instrumented with 4 pressure taps in the plane face and 5 pressure tapes distributed circumferentially in the transversal central-plane of the cylinder (-60°, -30°, 0°, +30°, +60°). Figure 3 illustrates the semi-circular cylinder and the pressure taps insertions.

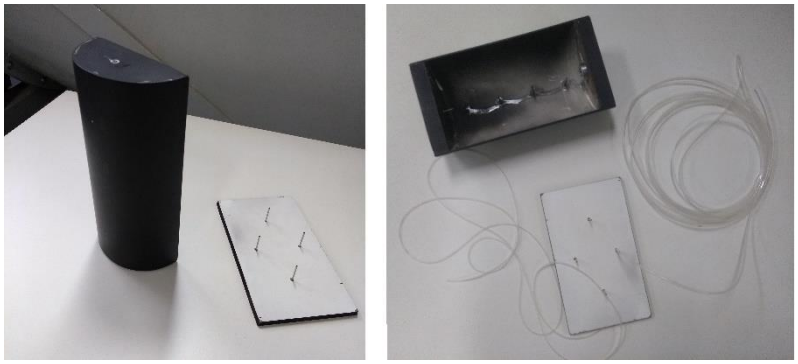

Figure 3. Test-article: wall mounted semi-circular cylinder with aspect ratio 2.

Drag measurements for the semi-circular cylinder was carried out using a 3-component (lift-drag-moment) aerodynamic balance fixed in the lateral of the TV-60. The cylinder has been fitted to the balance main axle and positioned very close to the side-panel of the wind tunnel. Fig.4 illustrates the fixation of the cylinder in the balance and the gap between the cylinder and the wind tunnel sidewall. The aerodynamic balance is controlled by software-interface where the values of kilogram-force are displayed for all configurations tested. The wind tunnel was set in the desired speed (16 m/s) and ten (10) measurements were taken. This process was repeated two more times, having an average of 10 measurements at each time and finally an average of 3 trials.

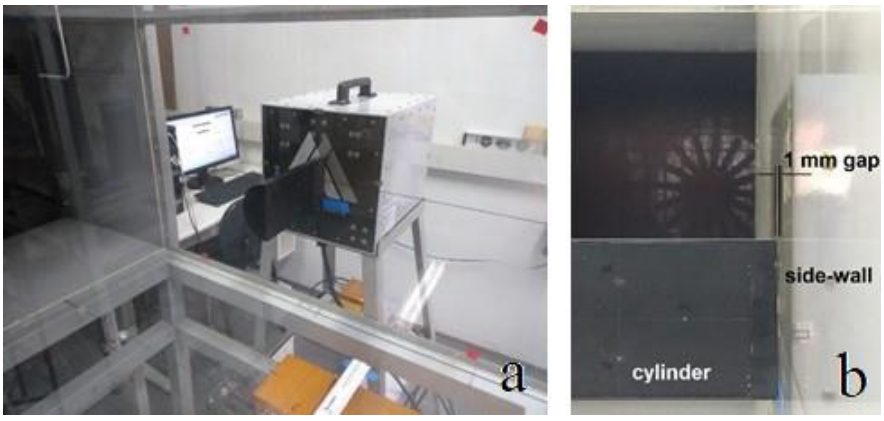

Figure 4. (a) 3-component aerodynamic balance; (b) cylinder assembly.

The pressure measurements were performed with a 64-channel pressure transducer module AA-TVCR2®. This module was designed to receive static pressure and total pressure (differential pressure). The differential pressure is then measured, having as the reference the static pressure inside the test-section. Before starting the acquisition, a simple calibration check was performed against measurements with a Pitot tube.

3. NUMERICAL MODELLING

The numerical setup and simulations were performed at the Fluid Mechanics and Mass Transfer Laboratory from Faculty of Mechanical Engineering (FEIS-UNESP). As a first approach a commercial code was applied – ANSYS Fluent®. The licenses and computational resources were provided by CPAERO at the time of this study. However, the next steps of this ongoing research are to apply in-house/open codes such as OPENFOAM® to solve the flow around finite height semi-circular cylinders. Following, it is described all the procedures taken for the simulation:

3.1 Computational domain and boundary conditions

The flow domain sizing was based on the cylinder diameter (D). The experimental flow condition has been considered with a Reynolds number of 9.34 x 10^4 and the aspect ratio (AR) equal to 2. Figure 5 describes the size of the computational domain used for the RANS and simulation.

The circular cylinder surface was treated as a viscous wall with no slip boundary condition. The inflow boundary condition was set at the entry of the computational domain while the opposite side boundary was set as outflow boundary condition. The turbulence level at the inlet boundary condition was 2%. The top and the sides of the computational domain were treated as symmetry. The bottom of the computational domain was taken as a wall with no slip condition, as seen in the experimental wind tunnel approach.

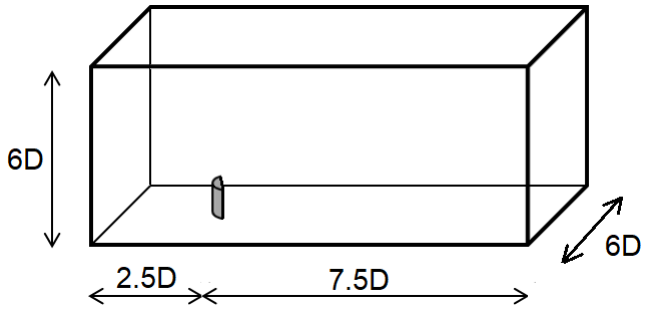

Figure 5. Exemplification of the size of the computational domain used for simulation

It is important to emphasize that the size of the computational domain was evaluated by previous simulations – not shown herein for brevity – and it's considered that the results are minimally affect by the boundary conditions. Also, a check for the mesh resolution was tried by using three different sizes. The best combination of domain size and mesh resolution is presented.

3.2 Mesh resolution

The mesh used in this study were generated in the grid generator ANSYS Icemcfd®. A refined mesh was considered for the steady-state Reynolds-Averaged Navier-Stokes approach via k-ω SST turbulence modeling (see Fig 6). Later, the code ANSYS Fluent® CFD has been applied to the analysis, considering the same meshes and setup. The number of each cell type is presented in Tab. 1 and the total amount of elements was 2579328.

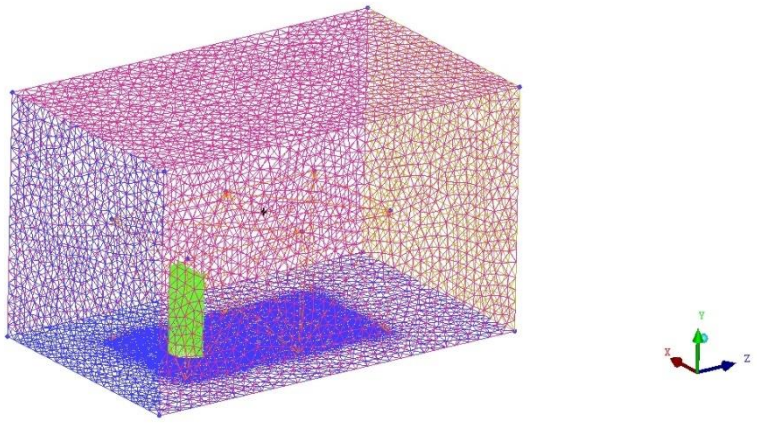

Figure 6. Computational domain, unstructured tetrahedral mesh elements.

Table 1. Number of each type of mesh elements

Element type	**Number of cells**
Tetrahedral	2533866
Triangular	20598
Pentagonal	24496
Quadratic	368

The next section is devoted to present the results according to the approach considered herein, starting with general experimental data from flow characterization, flow visualization, drag measurement and pressure distribution. As said earlier, these are preliminary data and additional investigation is being developed as a continuation of this research.

4. RESULTS AND DISCUSSION

4.1 Boundary Layer

Figure 7 shows the normalized velocity-profile for the wind tunnel boundary layer development upstream of the finite-height semi-circular cylinder at location x/D = -2 (the origin is placed at the bottom part of the front-face of the body). The plot was obtained with a hot-wire anemometer placed in x/D = -2 and moving it vertically with an empty test section. The measurements were performed for the ground from 2 mm up to 150 mm. The test was conducted for the velocity of U_∞ = 16.0 m/s. According to the results the boundary layer thickness is around an average of 4.0 mm.

Some boundary layer parameters from this experiment was calculated and presented on Table 2. The obtained shape factors are typical of turbulent boundary layers, according to classical literature (White, 2003), and is consistent with the Reynolds number flow regime analyzed in this work.

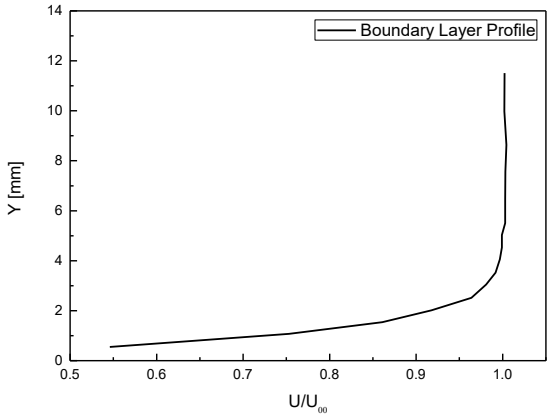

Figure 7. Normalized profile for the boundary layer at x/D = -2.

Table 2. Boundary layer calculated parameters.

U_∞ [m/s]	Layer Thickness	Displacement thickness	Momentum thickness	Shape factor
	δ [mm]	δ* [mm]	θ [mm]	H = δ*/θ
16.00	3.0	0.3801	0.2830	1.3431

Thus, it was assumed that this result was consistent and could be further applied for improving numerical simulations by applying such velocity profiles at the inlet condition in the computational domain.

Another important variable for this kind of experiment is the turbulent intensity defined as:

$$I_{turb} = \frac{U_{RMS}}{U_0} \tag{1}$$

The turbulent intensity was around 0.81% for the velocity investigated in this work.

4.2 Flow field

Previous works pointed out to the complexity of the 3D-flow over surface-mounted circular cylinders (Sumner, 2013). To obtain a general overview of the flow field around the finite-height semi-circular cylinder, both experimental and numerical flow visualization were considered. In the wind tunnel, by means of a smoke generator, it was possible to provide a quick overview about the flow pattern. On the other hand, the numerical simulations allowed a more deeply understanding of the flow field by means of plotting the velocity vectors and contours as well as path lines. The idea was to compare directly both numerical and experimental data to represent the flow over the top and bottom part of the semi-circular cylinder, these results are shown in Fig. 8 and Fig. 9.

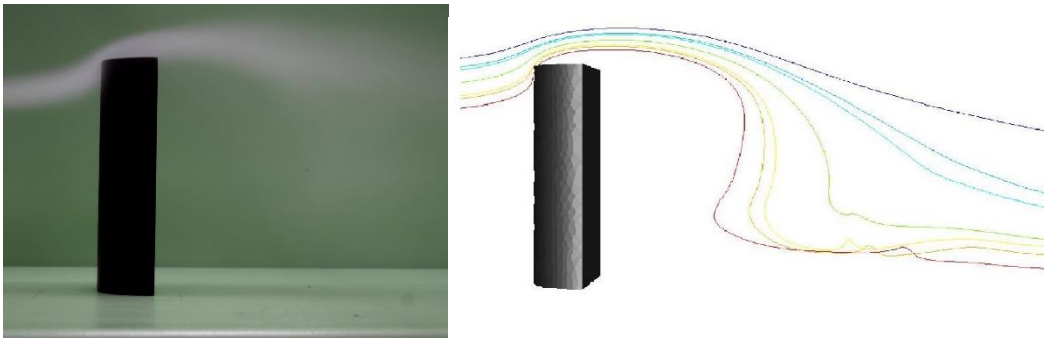

Figure 8. Path lines from the flow field around the semi-circular cylinder top part.

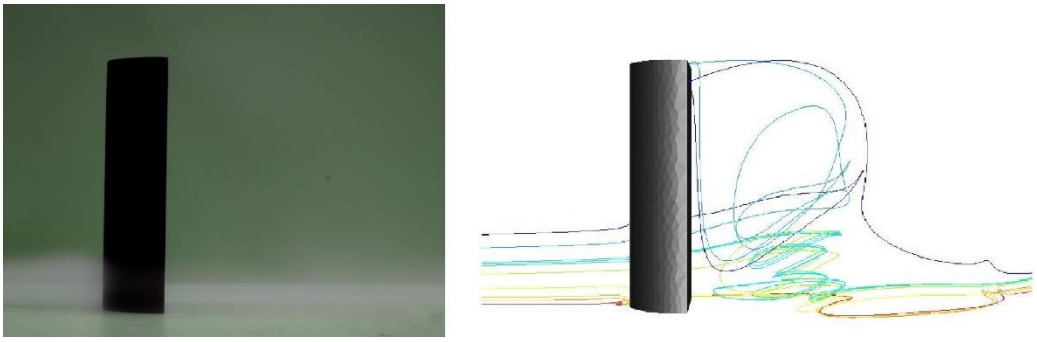

Figure 9. Path lines from the flow field around the semi-circular cylinder bottom part.

Even though the visualization with the use of smoke did not provide a clear detail of the flow pattern in the wake of the body, it is possible to assume a complex flow at that location which was confirmed by the numerical path lines. A 3D-flow was identified with a rolling of strong vortices downstream the cylinder leading to secondary recirculation zones behind the flat-face.

To help in a better understanding of this flow pattern, Fig. 10 shows a top view image and a perspective view of the path lines obtained numerically.

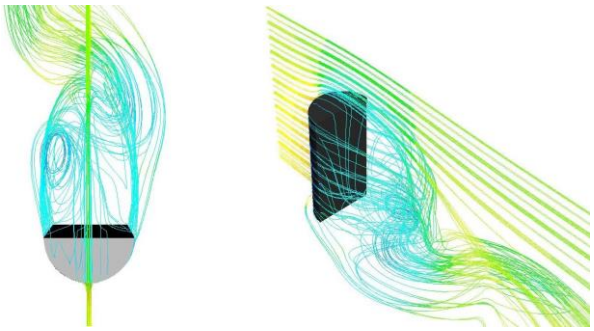

Figure 10. Top and perspective views of path lines from the flow field around the semi-circular cylinder.

The top and perspective views of the path lines by CFD confirm the complex flow around the semi-cylinder, it was possible to identify the recirculation and massive separations formed in the wake region behind the semi-

circular cylinder. Likewise, the work of Frederich et al. (2007), who also proposed a model based on numerical simulations of the flow around a finite cylinder of AR = 2 and Reynolds number of 2×10^5, similar characteristics of the flow behavior were obtained on this studied of the semi-cylinder – Fig.11. In both models were able to see side-tip vortices generated from the sides of the free-end surface, recirculation arch vortex with a tornado like region behind the semi-cylinder and horse-shoe vortex.

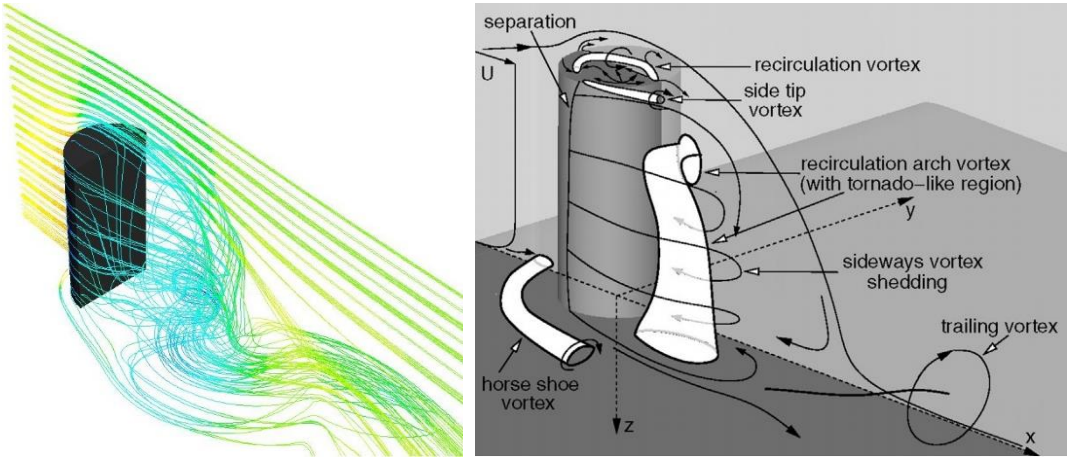

Figure 11. Comparison of the flow field – semi-circular and circular cylinder (reference: Frederich et al. (2007)).

Finally, velocity vectors representing the flow field over the semi-circular cylinder is shown in Fig.12. It was observed that the flow velocity was decelerated in the front when passing the cylinder, and then, the velocity of the flow was accelerated at the cylinder tips, producing jet flow.

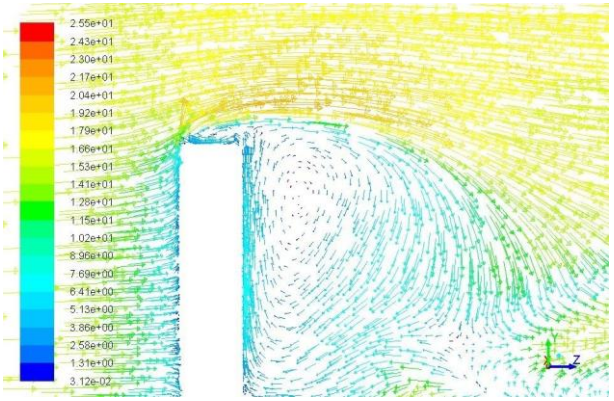

Figure 12. Velocity vectors from the flow field around the semi-circular cylinder

The flow field adjacent to the cylinder wall is strongly accelerated and at some positions several distances from the cylinder. However, this behavior is not present close to the junction wall where the acceleration magnitude is significantly smaller. It seems that there is an interaction between the detaching horse-shoe vortices from the junction affecting the periodic shedding vortices from the cylinder, increasing the complexity of the flow. Due to the complexity of this flow, additional and more sophisticated analyses must be performed both experimentally and numerically to improve the characterization of the flow field – steps for future work.

4.3 Drag Coefficient

As pointed out in the work of Merrick and Bitsuamlak (2008), when simulating the wind flow over a scale model comprised of curved surfaces, discrepancies are present between the model scale data and full-scale winds experienced by the structure. Moreover, subcritical flow over a smooth cylinder generally occurs at Re less than 2×10^5. Sub-critical flows are characterized by laminar flow over the windward surface of the cylinder with the flow separating on the upwind face. Super-critical flow occurs at Re greater than 4×10^6 and is evident by the turbulent boundary layer that forms over the surface of the cylinder. The turbulent wind separates from the cylinder

on the leeward face and results in a lower drag coefficient. The critical region is defined as flow resulting at Re between those of sub-critical and super-critical flows. Based on this assumption, it is believed that the flow regime undertaken is on this situation, leading to drag coefficients between 0.5 and 1.1, as presented in the literature.

Table 3 presents the drag coefficient obtained in this work by considering experimental and numerical measurements. The drag coefficient in this study (C_D = 0.838) was a little bit higher than the results obtained in the literature data as pointed in the work of (Kawamura et al., 1984) for full-circular cylinders, where drag coefficient was 0.78. As previously seen, the drag coefficients were obtained experimentally by a 3/8-inch screw thread assembled at the base of the semi-circular cylinder to give the access to the axis of the aerodynamic 3-component balance for measuring the drag force.

Table 3. Drag coefficient evaluation.

Experimental	Numerical
0.838	0.824

The numerical data for drag coefficient has been running for 5000 iterations with a convergence in the drag coefficient of value 0.824, very close to the value found experimentally, an error between the two results of 1.7%. Table 4 illustrate a summary of the ANSYS Fluent® Force reports, showing the converged value for the drag coefficient.

Table 4. Summary of the force reports.

Zone	Coefficients		
	Pressure	Viscous	Total
Cylinder	0.809	0.014	0.824
Net	0.809	0.014	0.824

4.4 Pressure Distribution

The pressure distribution was also made by considering the flow regime investigated in this work. According to previous historical data, the theoretical Cp-distribution was plotted against experimental data for a circular cylinder exposed in a subcritical and supercritical flow regime, Anderson (2011). Both experimental and numerical data for the forward face, by considering the angles 0°, +30° and +60°. All these data are shown in Fig. 13.

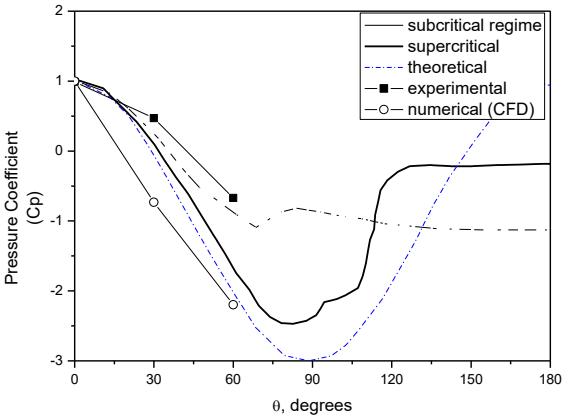

Figure 13. Cp-distribution over a circular cylinder in low-speed flow. Comparison of the theoretical pressure distribution with experimental and numerical data. Adapted from Anderson (2011).

The experimental pressure distribution in the forward face was close to the subcritical data from literature, clearly showing the influence of the Re number in this study. However, what was surprising were the data gathered from the numerical simulation, following a different trend, more closely to the supercritical and theoretical curves. It should be noted here that the flow pattern, consequently, wake behavior and drag on the cylinder is dependent of the pressure distribution. The difference in the numerical and experimental data in terms of pressure distribution could not be explained at the time of this study. It was proposed a new set of numerical simulations for investigating this trend.

5. CONCLUDING & REMARKS

The flow field characteristics around a semi-circular cylinder of finite height with aspect ratio (AR) of 2 was investigated both numerically and experimentally. Preliminary results were satisfactory and consistent with other data from literature. Some questions arose about the pressure distribution over the cylinder forward face and it was proposed a new set of numerical simulations to tackle such a problem.

Despite the lack of agreement in the cp-distribution in the cylinder surface, the numerical data for C_D was in agreement with the experimental value of 0.838. Also, the general flow field, mainly identified by CFD data, presented the same flow structures as seen in the flow over a circular cylinder and illustrated by Frederich et al. (2007).

The next steps for this study are listed as follows:

Experimental approach:

- To improve the sizing and installation of the pressure taps in the surface of the cylinder. Also, to include more pressure points;
- To visualize the flow field by using other experimental techniques such as oil-flow or china-clay;
- To test the effect of boundary layer and Re number.

Numerical approach:

- To verify the effect of post-processing in the data, especially in the cp-distribution;
- To use open-source code such as OpenFoam® for redoing all simulations tested so far;
- To enhance flow field visualization by using other computational criteria;
- To change to more realistic simulations by employing transient (unsteady) flow analysis (this will require more computational resources).

6. Acknowledgements

The first author would like to thank the Fluid Mechanics and Heat Mass Transfer Laboratory (FEIS-UNESP) for supporting the development of this work and for funding the participation on this event. Also, many thanks for Experimental Aerodynamics Research Center (CPAERO) from Federal University of Uberlandia for providing part of the computational resources.

7. REFERENCES

Adaramola, M., Akinlade, O., Sumner, D., Bergstrom, D. and Schenstead, A., 2006. “Turbulent wake of a finite circular cylinder of small aspect ratio”. *Journal of Fluids and Structures*, Vol. 22, No. 6-7, pp. 919–928.

Anderson Jr, John David. Fundamentals of aerodynamics. Tata McGraw-Hill Education, 2011.

Elbatran, A.H., 2016. “Des of the turbulent flow around a circular cylinder of finite height”. *Journal of Naval Architecture and Marine Engineering*, Vol. 13, No. 2, pp. 179–188.

Frederich, O., Wassen, E., Thiele, F., Jensch, M., Brede, M., Hüttmann, F. and Leder, A., 2007. “Numerical simulation of the flow around a finite cylinder with ground plate in comparison to experimental measurements”. In *New Results in Numerical and Experimental Fluid Mechanics VI*, Springer, pp. 348–355.

Johnston, C. and Wilson, D., 1997. “A vortex pair model for plume downwash into stack wakes”. *Atmospheric Environ- ment*, Vol. 31, No. 1, pp. 13–20.

Kawamura, T., Hiwada, M., Hibino, T., Mabuchi, I. and Kumada, M., 1984. “Flow around a finite circular cylinder on a flat plate: Cylinder height greater than turbulent boundary layer thickness”. *Bulletin of JSME*, Vol. 27, No. 232, pp. 2142–2151.

Merrick, R., Bitsuamlak, G., 2008 "Control of flow around a circular cylinder by the use of surface roughness: A computational and experimental approach." *Proceeding of the 4th International Conference Advances on Wind and Structures* (AWAS08), Jeju.

Pattenden, R., Turnock, S. and Zhang, X., 2005. “Measurements of the flow over a low-aspect-ratio cylinder mounted on a ground plane”. *Experiments in Fluids*, Vol. 39, No. 1, pp. 10–21.

Sumner, D., 2013. “Flow above the free end of a surface-mounted finite-height circular cylinder: a review”. *Journal of Fluids and Structures*, Vol. 43, pp. 41–63.

Tsutsui, T., 2012. “Flow around a cylindrical structure mounted in a plane turbulent boundary layer”. *Journal of Wind Engineering and Industrial Aerodynamics*, Vol. 104, pp. 239–247.

White, Frank M. "Fluid mechanics." McGraw-Hill, New York, NY 10020 (2003).